Self-trapping of the N–H vibrational mode in α-helical polypeptides

Dmitry V. Tsivlin[a] and Volkhard May
Institut fur Physik, Humboldt-Universität zu Berlin, Newtonstraße 15, D-12489 Berlin, Germany

(Received 5 September 2006; accepted 3 November 2006; published online 8 December 2006)

Recent calculations on the formation of self-trapped amide group vibrational states in α-helical polypeptides [J. Chem. Phys. **124**, 134907 (2006)] are extended to the amide N–H normal mode vibrations. First, the adiabatic N–H vibrational single- and two-exciton states are examined by treating the longitudinal chain coordinates as parameters. Then, in using the multiconfiguration time-dependent Hartree method coupled exciton-chain vibrational quantum dynamics are accounted for. Based on the respective exciton-chain vibrational wave function propagation the infrared transient absorption related to a sequential pump-probe experiment is calculated. The modulation of local amide vibrational energies by the longitudinal chain coordinates is found to have a pronounced effect on the broadening of absorption lines. Moreover, the ultrafast exciton transfer in the system is studied in order to characterize the dynamics of the self-trapped single-exciton states on a time scale below 10 ps. © *2006 American Institute of Physics*. [DOI: 10.1063/1.2402171]

I. INTRODUCTION

The ongoing progress in the field of ultrafast infrared spectroscopy has brought new interest to the studies of ultrafast vibrational dynamics in biologically relevant molecular systems (see, for example, Refs. 1–3) also initiating various accompanying theoretical simulations, e.g., Refs. 4 and 5. In particular, the long-standing debate on the existence of self-trapped vibrational states in α-helical polypeptides has been reanimated. Following the idea of the so-called Davydov soliton proposed some three decades ago exciton self-trapping in these systems has been extensively studied theoretically (see Ref. 6 for an overview). However, an experimental proof for the existence of self-trapped states in α-helices has been lacking until recently. Using infrared femtosecond spectroscopy Ref. 7 has reported on the observation of self-trapped N–H first overtone stretching vibrations in dissolved poly-γ-benzyl-*L*-glutamate helices. The interpretation of the transient absorption spectra (TAS) was mainly based on recent theoretical works of Refs. 8–11. Within a linear chain model[8,9] as well as a three-dimensional model[10,11] of an α-helical polypeptide vibrational single- and two-exciton self-trapped states have been obtained assuming a coupling to low-frequency longitudinal helix vibrations. The two energetically lowest two-exciton self-trapped levels could be assigned to the observed peaks in the excited state absorption part of the TAS presented in Ref. 7.

While the approach of Refs. 8–11 directly aims at a calculation of the spectrum of the high-frequency amide group vibrations dressed by low-frequency longitudinal helix vibrations we suggested in Refs. 12 and 13 an alternative computational scheme. Instead of carrying out different approximate canonical transformations of the original Hamiltonian we, first, computed the adiabatic single- and two-exciton states of the system. They follow as overall eigenstates but with the longitudinal helix coordinates treated as parameters. These types of calculations resulted in an approximate picture of the spectrum with the focus on single and double amide I excitations in Refs. 12 and 13. In a second step, the results have been improved by a numerically exact solution of the complete time-dependent Schrödinger equation. The nonadiabatic effects in nonlinear infrared spectra have been recently studied in Ref. 14 for a peptide model system of two amide groups. To study a sufficiently long chain we did not perform calculations for the three-dimensional (3D) helix structure but considered a model for one of the three linear chains of hydrogen bonded amide groups. Then, up to nine low-frequency coordinates of the longitudinal amide group displacements could be considered. To reduce the computational effort the interaction with the solvent has been introduced via an overall effective dephasing time. In the case of a single amide unit a detailed study of solvation effects in nonlinear infrared spectra of peptides were done in Ref. 15.

A numerical solution of the Schrödinger equation became possible by using the multiconfiguration time-dependent Hartree (MCTDH) method.[16–19] Within this method the total wave function is represented as a time-dependent superposition of products of time-dependent single coordinate wave functions (time-dependent Hartree products). Based on the Dirac-Frenkel variational principle, equations of motion are formulated for the expansion coefficients as well as for the single coordinate wave functions. Since the latter depend on time, they may be adapted to the full wave function, thus drastically reducing the numerical effort compared to a standard basis-set expansion with time-independent functions.[19]

The energetically lowest single- and two-exciton states could be determined via imaginary time propagation done within the MCTDH method. Real time propagation of the complete wave function enabled us to obtain the linear absorption spectrum and the TAS. This has been achieved in using the time-dependent formulation of the absorption spectra. It offers the complete set of single- and two-exciton

[a]Electronic mail: tsivlin@physik.hu-berlin.de

states coupled to the longitudinal helix vibrations together with the oscillator strengths of linear and excited state absorptions. Therefore, our treatment also improves the studies of Refs. 8–11. Besides the description of transitions into the different exciton levels our calculations also account for the multitude of satellites related to the longitudinal chain vibrations. Thus, a more realistic description of what has been observed in the experiment could be achieved.

To be ready for a more direct comparison with the results of Ref. 7 we describe here the self-trapping of the amide N–H stretching mode and related linear and transient absorptions. As compared to the amide I vibration studied in Refs. 12 and 13 it is characterized by a larger anharmonicity A and a weaker interamide group electrostatic coupling J, with both values favoring vibrational self-trapping. To start our discussion Sec. II shortly recalls the main features of the model (for details see Appendix A and Ref. 13). Adiabatic single- and two-exciton levels are described in Sec. III. Section IV specifies details of the TAS computation. In addition to Ref. 12 Sec. V offers some results on the N–H vibrational excitation energy motion through the helix. The whole discussion is finalized with some concluding remarks in Sec. VI.

II. THE MODEL HAMILTONIAN

Infrared pump-probe experiments at polypeptides in the range of the local amide mode absorption result, at least, in the population of the first amide vibrational overtone state. Therefore, as in the case of electronic Frenkel excitons it is advisable to introduce an expansion with respect to the number of amide excitations and their spatial localization in the helix. The whole procedure as well as the detailed structure of the resulting Hamiltonian has been described in Ref. 13. Here, we only mention the central features (some more details on the Hamiltonian can also be found in Appendix A).

First, we introduce the wave function of the local high-frequency amide group excitations (e.g., amide I, amide II, or N–H excitation). It is denoted by $\chi_{m\mu}$ with m labeling the position of the amide group in the chain and $\mu=0$, 1, and 2 being the vibrational quantum number. The related energies are $E_{m\mu}$ (the m dependence is of only formal character here since any energetic inhomogeneity will be neglected in what follows). Product states referring to the excitations in the whole polypeptide are written as $\Pi_m \chi_{m\mu_m}$. An ordering of these states with respect to the number of basic excitations starts with the overall ground state

$$|0\rangle = \prod_m |\chi_{m0}\rangle. \tag{1}$$

The presence of a single excitation at unit m in the system is characterized by

$$|\phi_m\rangle = |\chi_{m1}\rangle \prod_{k\neq m} |\chi_{k0}\rangle, \tag{2}$$

whereas a doubly excited state may cover a double excitation of a single amide unit as well as the simultaneous presence of two single excitations at two different units,

$$|\tilde{\phi}_{mn}\rangle = \delta_{m,n}|\chi_{m2}\rangle \prod_{k\neq m} |\chi_{k0}\rangle + (1-\delta_{m,n})|\chi_{m1}\rangle|\chi_{n1}\rangle \prod_{k\neq m,n} |\chi_{k0}\rangle. \tag{3}$$

To describe existing experiments it is not necessary to introduce triple or quadruple excitations. The presented types of states form the so-called *exciton manifolds*.

An expansion of the complete Hamiltonian (including the coupling to the radiation field) with respect to these different excited states is written here as an ordering with respect to the ground state ($N=0$) as well as the single- and two-exciton manifolds ($N=1$ and $N=2$, respectively). Introducing respective projection operators $\hat{P}_N$ we write

$$H = H_0\hat{P}_0 + H_1\hat{P}_1 + H_2\hat{P}_2 - \mathbf{E}(t)[\hat{\boldsymbol{\mu}}_{10} + \hat{\boldsymbol{\mu}}_{21} + \text{H.c.}]. \tag{4}$$

H_N describe the complete intramanifold dynamics. They include the electrostatic coupling among different amide groups which are responsible for the amide excitation energy motion through the whole chain. The couplings cover the quantity J which describes the deexcitation of the first excited state of a given amide group and the excitation of one of the two nearest-neighbor amide groups from its ground state. Similar transitions from the overtone state down to the first excited state accompanied by an excitation of a neighboring amide group from the ground state into the first excited one are accounted for by $\tilde{J}$ (see Appendix A). Note that any assumption of a, e.g., dipole-dipole interaction type of this coupling is not necessary here. We also stress that a possible long-ranged character of the electrostatic couplings has only a weak influence on the multiexciton spectra and can be neglected.

Moreover, H_N account for the presence of low-frequency chain vibrations as well as their coupling to the local high-frequency amide group vibrations. The low-frequency motion is assumed to be harmonic and will be characterized by longitudinal displacements x_m of the various amide groups with respect to their equilibrium position [see Eq. (A2), the whole set of coordinates x_m is abbreviated by x]. The coupling of the x_m to the local high-frequency amide group vibrations is taken in a linear form, i.e., the energies E_{m0}, E_{m1}, and E_{m2} are modulated according to $E_{m0}+w_{m0}(x_m-x_{m-1})$, $E_{m1}+w_{m1}(x_m-x_{m-1})$, and $E_{m2}+w_{m2}(x_m-x_{m-1})$, respectively. This form is particularly suited for the coupling of the N–H excitations to amide group displacements. Once the distance of an amide group m to its left neighbor decreases the N–H excitation energy decreases also. As described in Ref. 13 concrete values for the w_{m0}, w_{m1}, and w_{m2} can be deduced from the general coupling scheme $\chi Q_m^2(x_m-x_{m-1})/2$ where Q_m are N–H vibrational coordinates and χ represents an overall coupling constant.

In a consequent expansion Eq. (4) should comprise intermanifold couplings such as H_{10}. It could be shown in Ref. 13, however, that they are only of marginal importance justifying their neglect here. Of course, intermanifold couplings have to be considered in relation to infrared excitations (with electric field strength $\mathbf{E}$). The dipole operator $\hat{\boldsymbol{\mu}}_{10}$ ($\hat{\boldsymbol{\mu}}_{01}$) describes ground-state single-exciton manifold transitions and

$\hat{\boldsymbol{\mu}}_{21}$ ($\hat{\boldsymbol{\mu}}_{12}$) those between the single-exciton and two-exciton manifolds (direct transitions from the ground state into the two-exciton manifold are negligibly weak).

To further specify the considerations to the amide N–H vibrational states in an α helix we shall use the following parameters. For the basic excitation of the N–H mode we set $E_{m0}=0$ and set the energy $E_{m1}=3520\ \mathrm{cm}^{-1}$. The energy of the first overtone is introduced as $E_{m2}=2E_{m1}-2A$ in using the anharmonicity constant A of $60\ \mathrm{cm}^{-1}$.[7] The interamide unit interaction constant J appearing in H_1 [Eq. (A3)] and H_2 [Eq. (A4)] amounts to $J=5\ \mathrm{cm}^{-1}$.[7] The quantity $\tilde{J}$ which additionally enters H_2 [Eq. (A4)] is taken to be equal to $\tilde{J}=7.2\ \mathrm{cm}^{-1}$. For the N–H excitation-chain vibration coupling constants [cf. Eqs. (A2), (A5), and (A6)] we take the values $w_{m0}=110$ pN, $w_{m1}=360$ pN, and $w_{m2}=660$ pN. These values are in line with the available data for the N–H amide vibration[7,20] and indicate a stronger coupling for higher excited amide states.[13] Again, identical parameters are assumed for all amide units in the chain, thus we shall neglect any effect of the chain inhomogeneity and disorder. The chain elastic constant is $W=13$ N/m and the amide unit mass is $M=114m_p$ (m_p stands for the proton mass). Absolute values of the transition dipole moments d_1 ($0\rightarrow1$ transition) and d_2 ($1\rightarrow2$ transition) are not necessary here. We only need their ratio d_2/d_1 which amounts to 1.426 (see Appendix A).

III. ADIABATIC VIBRATIONAL EXCITONS

Standard single- and two-exciton states are obtained by diagonalizing H_1-T_{vib} and H_2-T_{vib}, respectively (note the removal of the vibrational kinetic energy operator), and by fixing x at the ground-state equilibrium configuration x_0. These states are denoted as $|\alpha\rangle$ and $|\tilde{\alpha}\rangle$ and the corresponding energy eigenvalues as $\mathcal{E}_\alpha$ and $\mathcal{E}_{\tilde{\alpha}}$. If N_{amide} denotes the number of amide units in the chain we obtain N_{amide} single-exciton states and $N_{\mathrm{amide}}(N_{\mathrm{amide}}+1)/2$ two-exciton states.

By removing the restriction of the chain vibrational coordinates to x_0 while carrying out the diagonalization one arrives at the following so-called adiabatic exciton states (cf. Refs. 12 and 13):

$$|\Phi_\alpha^{(1)}(x)\rangle=\sum_m C_\alpha^{(1)}(m;x)|\phi_m\rangle \tag{5}$$

and

$$|\Phi_{\tilde{\alpha}}^{(2)}(x)\rangle=\sum_{m\leqslant n} C_{\tilde{\alpha}}^{(2)}(mn;x)|\tilde{\phi}_{mn}\rangle. \tag{6}$$

Now, the energy eigenvalues $\mathcal{E}_\alpha(x)$ and $\mathcal{E}_{\tilde{\alpha}}(x)$ as well as the expansion coefficients $C_\alpha^{(1)}(m;x)$ and $C_{\tilde{\alpha}}^{(2)}(mn;x)$ depend on the actual chain vibrational configuration x.

In order to find out whether or not self-trapped states are formed a multidimensional minimization of the single- and two-exciton energy levels versus the coordinates x has been performed. Respective results are displayed in Fig. 1 for single-exciton states and in Fig. 2 for two-exciton states. In Fig. 1 energy eigenvalues in the single-exciton manifold are drawn for a chain of ten amide units. The energies are calculated for the ground-state equilibrium chain configuration x_0 as well as for the relaxed configurations x_α. The latter

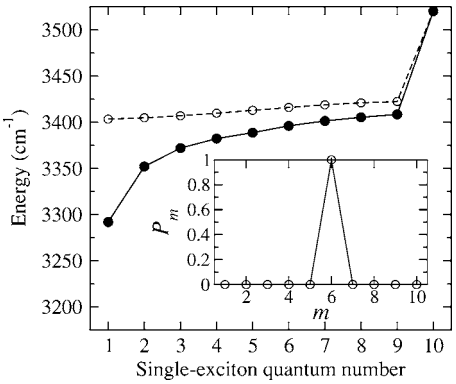

FIG. 1. Sequence of single-exciton energies for a chain of ten amide units vs the exciton quantum number $\alpha=1,\ldots,10$ (all energies are defined with respect to the minimum of the ground state PES). Open circles: $\mathcal{E}_\alpha$ at the chain equilibrium configuration x_0; full circles: $\mathcal{E}_\alpha$ at the relaxed chain configuration x_α. The inset shows the probability distribution P_m corresponding to the lowest single-exciton state $\alpha=1$.

correspond to the minima of the single-exciton energies $\mathcal{E}_\alpha(x)$. The asymmetric form of the coupling terms $w_{m1}(x_m-x_{m-1})$ in Eq. (A5) implies that for the first chain unit $m=1$ the excitation energy does not depend on the coordinates x_m. A local excitation of this first unit results in a higher-lying exciton state which is decoupled from the whole excitonic band (see Fig. 1, level $\alpha=10$). The differences $\mathcal{E}_\alpha(x_0)-\mathcal{E}_\alpha(x_\alpha)$ define respective reorganization energies λ_α. Moving to the lower part of the single-exciton band λ_α is significantly increased indicating self-trapping. The inset of Fig. 1 shows the probability distribution of amide group localized excitations along the chain,

$$P_m(\alpha)=|C_\alpha(m,x_\alpha)|^2, \tag{7}$$

as it is present in the lowest single-exciton state $\alpha=1$. It is essentially localized at one amide unit in the center of the chain.

Respective calculations for the two-exciton manifold are displayed in Fig. 2. In the case of the ground-state equilibrium chain configuration x_0 the two-exciton energy levels separate into three regions describing double on-site excita-

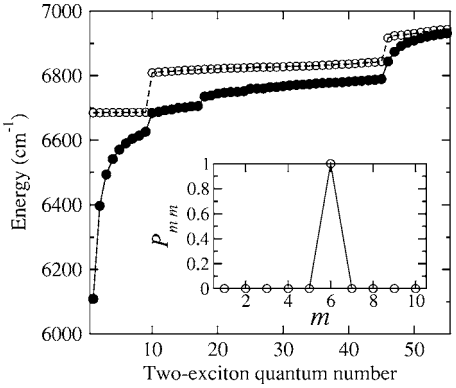

FIG. 2. Sequence of two-exciton energies for a chain of ten amide units versus the two-exciton quantum number $\tilde{\alpha}=1,\ldots,55$ (all energies are defined with respect to the minimum of the ground-state potential energy surface). Open circles: $\mathcal{E}_{\tilde{\alpha}}$ at the chain equilibrium configuration x_0; full circles: $\mathcal{E}_{\tilde{\alpha}}$ at the relaxed chain configuration $x_{\tilde{\alpha}}$. The inset shows the probability distribution P_{mm} corresponding to the lowest two-exciton state $\tilde{\alpha}=1$.

tions (low energy region), pairs of single excitations at different amide units (central energy region), and pairs of single excitations but involving the first unit of the chain (upper energy region). Upon chain relaxation the N–H overtone excitation of one amide unit in the center of the chain gives rise to the formation of the self-trapped two-exciton state $\tilde{\alpha}=1$. The inset in Fig. 2 shows the diagonal part of the two-site probability distribution

$$P_{mn}(\tilde{\alpha}) = |C_{\tilde{\alpha}}(mn,x_{\tilde{\alpha}})|^2 \tag{8}$$

for this state. Similar to the single-exciton case P_{mm} is localized at one central amide unit.

IV. TRANSIENT INFRARED ABSORPTION

A. Time-dependent multiexciton-chain vibrational states

The adiabatic exciton states [Eqs. (5) and (6)] are constructed in assuming the amide unit displacement coordinates x_m as continuously varying parameters. Hence, these states are not the eigenstates of the Hamiltonians H_1 or H_2. In order to achieve an entire quantum-mechanical description of the system we shall construct in the next step exciton-chain vibrational wave functions of the single- and two-exciton states as well as of the exciton ground state by solving the respective time-dependent Schrödinger equation. To obtain stationary lowest-energy exciton states, imaginary time propagation of the wave function in the respective exciton manifold may be used. Real time propagation of the wave function is carried out to obtain linear and transient infrared absorption spectra. Both are constructed by a Fourier transformation of appropriate wave function autocorrelation functions. As detailed in Ref. 13 the consideration of a sequential pump-probe experiment does not require any wave function propagation at the presence of the external infrared laser field. The numerical implementation of the wave function propagation is based on the MCTDH method.[21]

The computation of the complete exciton-chain vibrational wave function can be based on a basis-set expansion with respect to the adiabatic exciton states. However, since they are all related one to another by nonadiabatic couplings, it is rather advisable to use further the basis of local multiexcited amide states [Eqs. (1)–(3)]. Because our considerations are restricted to the amide ground state, as well as the manifolds of singly and doubly excited states, the expansion of an arbitrary state vector reads

$$|\Psi(t)\rangle = \psi_0(x,t)|0\rangle + \sum_m \psi_m(x,t)|\phi_m\rangle + \sum_{m\leqslant n} \tilde{\psi}_{mn}(x,t)|\tilde{\phi}_{mn}\rangle. \tag{9}$$

The expansion coefficients $\psi_0(x,t)$, $\psi_m(x,t)$, and $\tilde{\psi}_{mn}(x,t)$ have to be understood as wave functions of the longitudinal chain vibrations. They depend on the coordinates x and obey the following equations:

$$i\hbar\frac{\partial}{\partial t}\psi_0(x,t) = \langle 0|H_0|0\rangle\psi_0(x,t), \tag{10}$$

$$i\hbar\frac{\partial}{\partial t}\psi_m(x,t) = \sum_n \langle\phi_m|H_1|\phi_n\rangle\psi_n(x,t), \tag{11}$$

$$i\hbar\frac{\partial}{\partial t}\tilde{\psi}_{mn}(x,t) = \sum_{k\leqslant l} \langle\tilde{\phi}_{mn}|H_2|\tilde{\phi}_{kl}\rangle\tilde{\psi}_{kl}(x,t). \tag{12}$$

Since the equations have been set up at the absence of the laser field there only remains a coupling of all the $\psi_m(x,t)$ among each other and of all the $\tilde{\psi}_{mn}(x,t)$ among each other (in the MCTDH scheme this can be handled similar to nonadiabatic couplings between different electron-vibrational states).

B. Differential transient absorption spectra

The computation of the TAS referring to a sequential pump-probe experiment as described in Ref. 7 has been explained in Ref. 13. First, the weakness of the probe pulse offers the possibility to determine the probe pulse induced polarization linear with respect to the probe field $\mathbf{E}_{\mathrm{pr}}$. And second, because of the sequential character of the pump probe scheme the response function R_{pr} relating the probe pulse induced polarization to $\mathbf{E}_{\mathrm{pr}}$ can be calculated at the absence of the pump pulse. Because of the sequential character of the pump-probe scheme one can imply complete relaxation of the pump pulse induced excited state before the probe pulse starts to act. Such a relaxed excited state has been accounted for in Ref. 13 by introducing the following statistical operator:

$$\hat{W}_{\mathrm{rel}} = p_0|\Psi_0^{(\mathrm{rel})}\rangle\langle\Psi_0^{(\mathrm{rel})}| + p_1|\Psi_1^{(\mathrm{rel})}\rangle\langle\Psi_1^{(\mathrm{rel})}|, \tag{13}$$

which describes a mixed state of a depleted ground state and of some excitation in the single-exciton manifold. The latter is characterized by the following relaxed single-exciton chain vibrational wave function:

$$|\Psi_1^{(\mathrm{rel})}\rangle = \sum_m \psi_m^{(\mathrm{rel})}(x)|\phi_m\rangle, \tag{14}$$

and the first one by

$$|\Psi_0^{(\mathrm{rel})}\rangle = \psi_0^{(\mathrm{rel})}(x)|0\rangle. \tag{15}$$

Both are calculated by imaginary time propagation (see below). p_0 and p_1 denote the overall populations of the ground state and the manifold of singly excited states, respectively. Since higher excitations are neglected we have $p_0+p_1=1$, and either p_0 or p_1 has to be introduced as an external parameter to fix the excitation conditions.

If one uses $\hat{W}_{\mathrm{rel}}$ [Eq. (13)] to compute the response function R_{pr} one arrives at the following expression for the differential TAS:

$$\Delta S(\omega) = \frac{\omega_{\mathrm{pr}}V}{\pi}|E_{\mathrm{pr}}(\omega)|^2\,\mathrm{Im}\{R_{\mathrm{pr}}^{(\mathrm{GB})}(\omega+\omega_{\mathrm{pr}}) + R_{\mathrm{pr}}^{(\mathrm{SE})}(\omega+\omega_{\mathrm{pr}}) + R_{\mathrm{pr}}^{(\mathrm{EA})}(\omega+\omega_{\mathrm{pr}})\}, \tag{16}$$

where V denotes the sample volume and $E_{\mathrm{pr}}(\omega)$ is the Fourier-transformed probe pulse envelope. The expression includes Fourier-transformed response functions $R^{(\mathrm{GB})}$, $R^{(\mathrm{SE})}$, and $R^{(\mathrm{EA})}$ referring to the ground-state bleaching, the stimu-

lated emission, and the excited state absorption processes, respectively (see Ref. 13). They are defined as

$$R_{\mathrm{pr}}^{(\mathrm{GB})}(\omega) = -\frac{i}{\hbar} n_{\mathrm{pp}} p_1 \int_0^\infty dt e^{i(\omega+\Omega_{\mathrm{rel}}^{(0)})t - t/\tau_{\mathrm{deph}}} \times \sum_m \int dx d_1^* \psi_0^{(\mathrm{rel})*}(x) \psi_m(x,t), \tag{17}$$

$$R_{\mathrm{pr}}^{(\mathrm{SE})}(\omega) = -\frac{i}{\hbar} n_{\mathrm{pp}} p_1 \int_0^\infty dt e^{i(\omega-\Omega_{\mathrm{rel}}^{(1)})t - t/\tau_{\mathrm{deph}}} \times \int dx \sum_m d_1^* \psi_m^{(\mathrm{rel})}(x) \psi_0^*(x,t), \tag{18}$$

and

$$R_{\mathrm{pr}}^{(\mathrm{EA})}(\omega) = \frac{i}{\hbar} n_{\mathrm{pp}} p_1 \int_0^\infty dt e^{i(\omega+\Omega_{\mathrm{rel}}^{(1)})t - t/\tau_{\mathrm{deph}}} \times \sum_{m \leqslant n} \int dx (\delta_{m,n} d_2^* \psi_m^{(\mathrm{rel})*}(x) \tilde{\psi}_{mm}(x,t) + [1-\delta_{m,n}] d_1^* (\psi_m^{(\mathrm{rel})*}(x) + \psi_n^{(\mathrm{rel})*}(x)) \tilde{\psi}_{mn}(x,t)). \tag{19}$$

d_1 and d_2 denote the local dipole moments for the ground-state first-excited state transition and the first-excited state overtone state transition, respectively. $\hbar\Omega_{\mathrm{rel}}^{(0)}=44\ \mathrm{cm}^{-1}$ and $\hbar\Omega_{\mathrm{rel}}^{(1)}=3330\ \mathrm{cm}^{-1}$ are the energies of the ground state and the (relaxed) single-exciton state (lowest eigenvalues of H_0 and H_1, respectively). Moreover, n_{pp} is the volume density of polypeptides in the sample, and the factor $\exp(-t/\tau_{\mathrm{deph}})$ introduced under the time integral accounts for dephasing.

Before discussing the different parts of the TAS we shortly demonstrate the achieved accuracy of the MCTDH technique. This is done by considering the linear absorption spectrum of a single amide unit decoupled from all other ones (by setting J equal to zero), but interacting with the complete set of chain vibrations. Such an artificial situation is of interest since the absorption can be calculated alternatively in the framework of two harmonic potential energy surfaces (PESs) shifted with respect to each other (see, for example, Ref. 22). And indeed, we arrive at this standard model here if we change from the displacements x_m to normal mode coordinates of the chain (details can be found in Appendix B). The linear absorption, then, follows from a single Fourier transformation of an analytically known expression [cf. Eq. (B5)]. In contrast, the computation based on the MCTDH technique uses Eq. (17) for the ground-state bleaching part of the TAS (but here with $p_1=-1$). The respective spectrum is obtained in solving the coupled set of Eq. (11) for $\psi_m(x,t)$ with the initial conditions $\psi_m(x,0)=d_1\psi_0^{(\mathrm{rel})}$. The perfect agreement of both approaches is shown in Fig. 3.

After having done this particular check of the MCTDH technique we next directly calculate the ground-state bleaching part [Eq. (17)] in the way already described. In the case of the stimulated emission $\Sigma_m d_1^* \psi_m^{(\mathrm{rel})}$ serves as the initial condition for the propagation of $\psi_0(x,t)$ according to Eq. (10). A rather large number of coupled chain vibrational Schrödinger equations have to be solved in the case of excited state absorption (in the present case 55). One has to determine $\tilde{\psi}_{mn}(x,t)$ in using Eq. (12) and with the initial conditions $d_2\psi_m^{(\mathrm{rel})}(x)$ (for $m=n$) and $d_1[\psi_m^{(\mathrm{rel})}(x)+\psi_n^{(\mathrm{rel})}(x)]$ (for $m\neq n$).

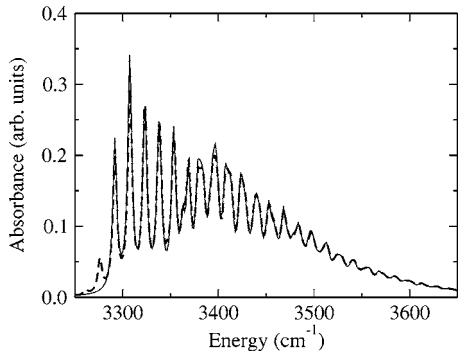

FIG. 3. Linear absorption spectrum of amide unit $m=6$ isolated from all other units by setting $J=0$ (chain of ten units and $\tau_{\mathrm{deph}}=2$ ps). Solid line: results based on two harmonic PESs; dotted line: results based on the MCTDH method.

Figure 4 shows the calculated spectrum of the ground-state bleaching part of the TAS [Eq. (17)]. Spectral broadening can be introduced according to the measured decay time of the amide vibration.[7] We use a dephasing time τ_{deph} of 2 ps. This value is somewhat larger than the measured one but guaranties the resolution of individual absorption lines. The low-energy part of the spectrum starts with the self-trapped single-exciton level (shown in Fig. 4 with an arrow). This level is accompanied by a sequence of absorption peaks originating from the coupling of the exciton to chain vibrations. The absorption maximum at 3520 cm^{-1} stems from the excitation of the first unit of the chain which does not couple to the chain coordinates. As it follows from the consideration of the adiabatic single-exciton states (cf. Fig. 1), the excitation of this unit (see energy level $\alpha=10$) is energetically separated from all other single-exciton states.

For the determination of the response functions $R_{\mathrm{pr}}^{(\mathrm{SE})}$ and $R_{\mathrm{pr}}^{(\mathrm{EA})}$ the relaxed single-exciton wave function (14) has to be calculated. To show the obtained result we introduce the time-dependent and full quantum dynamics based probability distribution of amide group localized excitations ($\int dx$ covers the integration with respect to all chain coordinates),

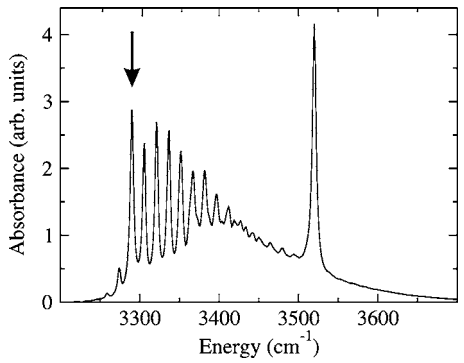

FIG. 4. Ground-state bleaching part $|\mathrm{Im}\, R_{\mathrm{pr}}^{(\mathrm{GB})}(\omega+\omega_{\mathrm{pr}})|$ of the TAS ($\tau_{\mathrm{deph}}=2$ ps).

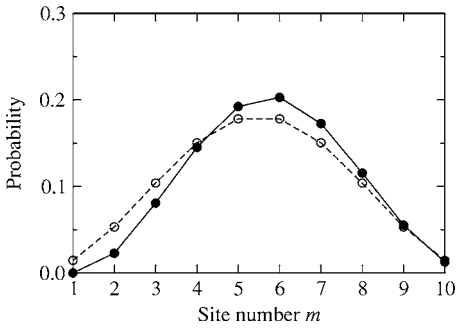

FIG. 5. Probability $P_m^{(\mathrm{rel})}$ to find a singly excited amide state at chain site m. Full circles: $P_m^{(\mathrm{rel})}$ corresponding to the relaxed single-exciton state; empty circles: distribution for the lowest exciton level in a rigid and regular chain.

$$P_m(t) = \int dx |\psi_m(x,t)|^2. \tag{20}$$

Changing from $\psi_m(x,t)$ to the relaxed state wave function $\psi_m^{(\mathrm{rel})}(x)$ introduced in Eq. (14) we arrive at the stationary distribution $P_m^{(\mathrm{rel})}$ shown in Fig. 5. Due to the exciton-chain vibrational coupling the distribution differs slightly from the standard result $P_m = 2/(N_{\mathrm{amide}}+1)\sin^2[\pi m/(N_{\mathrm{amide}}+1)]$ for the lowest exciton level in a rigid and regular chain. Note also the smallness of $P_1^{(\mathrm{rel})}$ which reflects the absence of any coupling to chain vibrations at this terminal amide unit. At the first glance the shape of $P_m^{(\mathrm{rel})}$ contradicts self-trapping as displayed for the lowest adiabatic single-exciton state in Fig. 1. The quantum description also of the longitudinal chain vibrations, however, results in a superposition of different adiabatic (self-trapped) two-exciton states localized at different amide units, thus, leading to a rather broad distribution $P_m^{(\mathrm{rel})}$ along the chain.

The stimulated emission signal is calculated in using Eq. (18) and is presented in Fig. 6. As it has to be expected the high-energy tail is positioned in the energy range of the low-energy tail of the ground-state bleaching spectrum (Stokes shift). Since amide unit $m=1$ does not contribute to the relaxed single-exciton state [Eq. (14)] the stimulated emission spectrum does not include a similar isolated peak as the ground-state bleaching signal at about 3520 cm^{-1}.

We now turn to the spectrum of the excited state absorption shown in Fig. 7. The low-energy part of the absorption band starts at the transition energy into the lowest two-

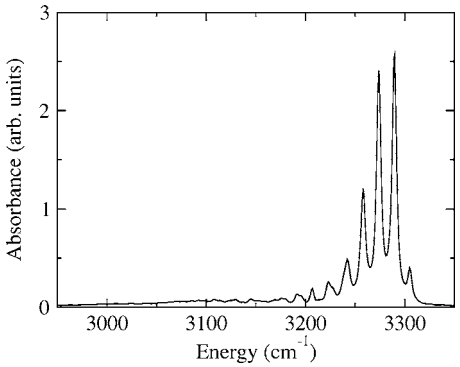

FIG. 6. Stimulated emission part $|\mathrm{Im}\, R_{\mathrm{pr}}^{(\mathrm{SE})}(\omega+\omega_{\mathrm{pr}})|$ of the TAS ($\tau_{\mathrm{deph}}=2$ ps).

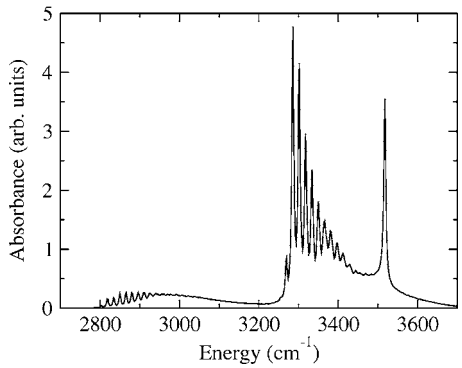

FIG. 7. Excited state absorption part $|\mathrm{Im}\, R_{\mathrm{pr}}^{(\mathrm{EA})}(\omega+\omega_{\mathrm{pr}})|$ of the TAS ($\tau_{\mathrm{deph}}=2$ ps).

exciton self-trapped state (cf. Fig. 2, state $\tilde{\alpha}=1$), and is followed by the progression of chain vibrational levels related to this state. As it follows from the spectrum of adiabatic two-exciton states (Fig. 2), $\tilde{\alpha}=2$ and $\tilde{\alpha}=3$ two-exciton levels may also contribute to this low-energy band of the excited state absorption. This point will be discussed below in more detail. Higher-lying two-exciton states and respective chain vibrational satellites form the remaining part of the excited state absorption spectrum. The isolated peak at 3520 cm^{-1} is originated by the participation of the first amide unit in the chain (which does not couple to chain vibrations).

The broadband originated by self-trapped two-exciton states also appears in the full TAS [Fig. 8(a)] (dephasing time $\tau_{\mathrm{deph}}=2$ ps). It dominates the energy range up to 3200 cm^{-1}. In the remaining part of the spectrum above 3200 cm^{-1} the interplay of all three contributions to the full TAS results in a rather complicated oscillatory behavior. Decreasing τ_{deph} down to a value of 0.3 ps [as shown in Fig. 8(b)] the low-energy band becomes more pronounced compared to the remaining spectrum. Resulting from the broadening of the $\tau_{\mathrm{deph}}=2$ ps spectrum two regions with a negative TAS are separated by a positive region around 3300 cm^{-1}.

To achieve a better understanding of this behavior we also calculated the TAS at the absence of any electrostatic coupling among the amide units ($J,\tilde{J}=0$). Moreover, a relaxed excited state concentrated at unit $m=6$ has been taken,

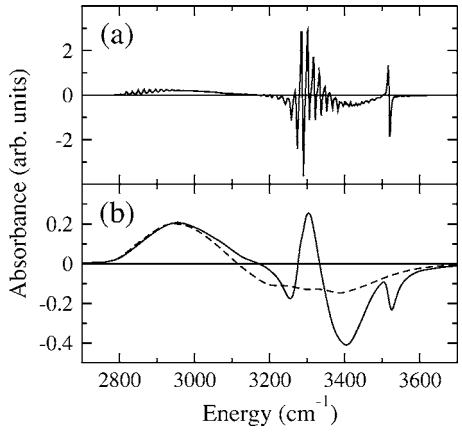

FIG. 8. Total frequency dispersed TAS. (a) $\tau_{\mathrm{deph}}=2$ ps and (b) $\tau_{\mathrm{deph}}=0.3$ ps. Solid line: $J, \tilde{J}\neq 0$; dashed line: $J, \tilde{J}=0$ (for more details see text).

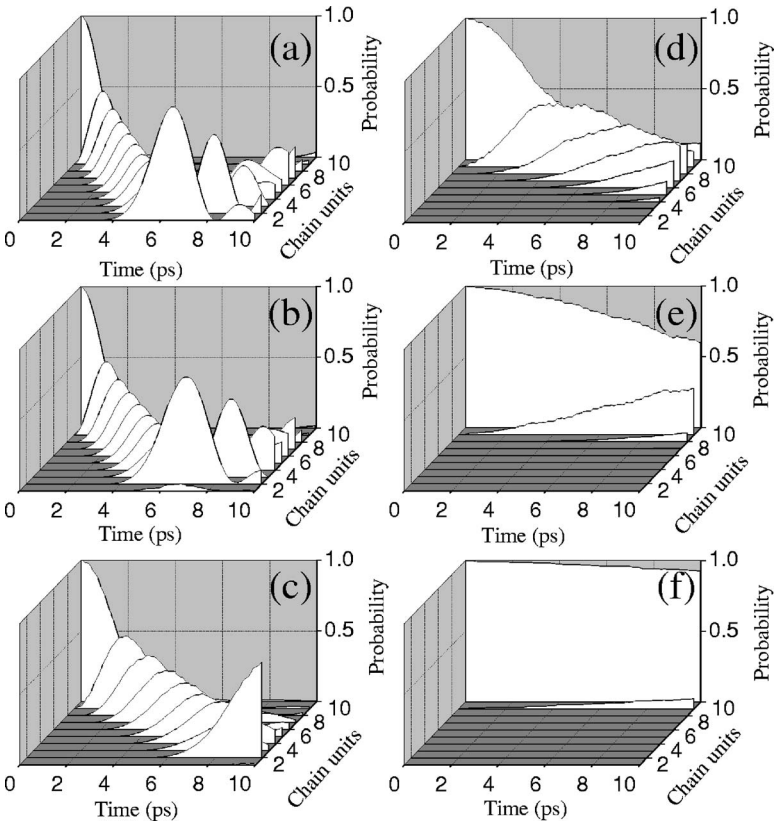

FIG. 9. Probability distributions $P_m(t)$ vs time for a chain of ten amide units and for different values of the exciton-chain vibrational coupling constant χ: (a) 0 pN, (b) 60 pN, (c) 120 pN, (d) 180 pN, (e) 240 pN, and (f) 300 pN.

i.e., we set $\psi_m^{(\mathrm{rel})}(x) \sim \delta_{m,6}$. As displayed in Fig. 8(b), now the region where self-trapped states contribute is somewhat decreased at the high-energy tail and it is followed by an energy range with an overall negative TAS.

Moving back to the original case with $J, \tilde{J} \neq 0$ we may state that in this situation the oscillator strength of the $1 \rightarrow 2$ transitions has been redistributed. Transitions into two-exciton states composed of two different singly excited amide units get enhanced oscillator strength. As a result the excited state absorption part of the TAS above 3200 cm^{-1} dominates the complete signal and leads to the second positive peak.

The presence of two positive bands in the TAS agrees with the recent experimental observations.[7] However, the given interpretation differs somewhat from our results. While it was argued in Ref. 7 that the two observed peaks correspond to distinct self-trapped two-exciton levels, we demonstrated that isolated two-exciton peaks cannot be expected. Instead, they are always accompanied by vibrational satellites of the longitudinal chain motion. Thus, our theory gives the correct line shape of the differential absorption. The broad positive band in the TAS located between 2800 and 3200 cm^{-1} predominantly corresponds to the absorption into the lowest two-exciton self-trapped state. This band is well reproduced in the case $J, \tilde{J}=0$ where the excitation of the first overtone amide level appears at a single unit coupled to the longitudinal chain vibrations [cf. Fig. 8(b), dashed line]. Also we expect that with increasing chain size progressions of vibrational satellites become more dense, while the contribution of the first decoupled amide unit at 3520 cm^{-1} decreases.

According to the experiment of Ref. 7 upon unfolding of the helical structure the hydrogen bonds between different amide units are destroyed. In this case the differential absorption spectrum shows no positive band in the low-energy range. In our model the effect of hydrogen bonds is described by the exciton-chain vibrational coupling $w_{m\mu}$ [cf. Eqs. (A5) and (A6)]. According to our test calculations (not shown) if this coupling is neglected the broadband around 3000 cm^{-1} in the TAS [Fig. 8(b)] disappears in agreement with the experimental observation.

V. ULTRAFAST EXCITON TRANSFER

As reviewed in detail in Ref. 6 the study of the amide unit excitation energy motion in α-helical polypeptides found much more interest compared to calculations of related infrared spectra. In relating our full quantum dynamical approach to this earlier tendency in theoretical literature, here, we study the motion of a single excitation in a linear chain of ten amide units in focusing on N–H vibrations. Therefore, we have performed a series of time propagations of the single-exciton chain vibrational wave function,

$$|\Psi_1(t)\rangle = \sum_m \psi_m(x,t)|\phi_m\rangle, \tag{21}$$

for different values of the exciton-chain vibrational coupling parameters χ (see Sec. II). $\psi_m(x,t)$ are obtained by the solution of Eq. (11), and the initial state is given by a single excitation completely localized at the terminal amide unit $m=10$. Moreover, the chain vibrational ground state is taken.

Figures 9(a)–9(f) show the obtained time-dependent probability distributions $P_m(t)$ [Eq. (20)] deduced from the

various $\psi_m(x,t)$ and for exciton-chain vibrational coupling parameters varying in the range from $\chi=0$ pN (free exciton propagation) to $\chi=300$ pN (strong self-trapping). In the case of small χ an excitonic wave packet moves freely from one chain end to the other. After its reflection subsequent dispersion may appear. Since the local amide levels at the first chain unit $m=1$ are not modulated by chain coordinates the respective excitation energy turns out to be higher than the energy of the states located in the remaining part of the chain. As a result, the self-trapped state wave packet becomes reflected from the first chain unit $m=1$ (note the case of $\chi=60$ pN in Fig. 9). With a further increase of χ the wave packet motion slows down and for the largest value $\chi=300$ pN considered here the amide excitation becomes essentially trapped at the initially excited unit of the chain within the time scale of the simulation.

Although the qualitative features of the described behavior have been reported already at different places earlier (see Ref. 6 for an overview) our approach represents a consistent quantum simulation of the exciton-chain vibrational dynamics. Moreover, for any approximate description necessary for larger systems the obtained results can be used as reference data.

VI. CONCLUSIONS

Interacting N–H vibrational normal mode excitations of amide units in α-helical polypeptides have been studied. Dealing with a model of one-dimensional chain of ten coupled amide units the focus has been put on the self-trapping of single- and two-exciton states formed by amide unit excitations. First, to obtain reference data self-trapping has been described in analyzing the spectrum of adiabatic single- and two-exciton states. These states and the related energies depend parametrically on the longitudinal displacement coordinates of the amide units in the chain. Both spectra if calculated for respective relaxed chain configurations show levels at their low-energy tail which are separated in a pronounced manner from the majority of higher-lying ones. In this scheme of adiabatic excitons the localization of excitation probability appears in one central unit of the chain. It is singly excited for a self-trapped single-exciton state. In the case of a self-trapped two-exciton state the first overtone of the central amide unit becomes excited.

To achieve the quantum description also of the longitudinal chain vibrations a time-propagation of the full wave function is performed in using the multiconfiguration time-dependent Hartree (MCTDH) method. Based on an imaginary time propagation the probability distribution of the amide unit overtone excitations has been computed. It refers to the lowest self-trapped two-exciton state but shows a broad probability distribution across the ten amide units. This results from a superposition of different adiabatic (self-trapped) two-exciton states localized at different amide units.

To apply the MCTDH method also for a computation of infrared transient absorption spectra (TAS) a respective time-dependent formulation has been used based on the computation of different exciton-chain vibrational correlation functions. A positive band in the low-frequency part of the TAS is found to be originated by transitions from the single-exciton manifold primarily into the lowest self-trapped two-exciton state. Since low-frequency longitudinal chain vibrations have been included, TAS covers chain vibrational satellites of the two-exciton levels leading to a significant broadening of the band.

Single-exciton states have been additionally characterized by calculating the time-dependent exciton probability distribution in the chain starting with an excitation of the terminal unit. This numerically exact description of the excitonic wave packet propagation has been performed for different strengths of the exciton coupling to chain longitudinal vibrations and should serve as a reference case for future approximate descriptions. Those are necessary when dealing with longer chains and if one takes into to account the 3D structure of the helix. The respective work is in progress.

ACKNOWLEDGMENTS

The financial support of the Deutsche Forschungsgemeinschaft through Project No. Ma 1356/8-1 is gratefully acknowledged. We also thank H.-D. Meyer for the assistance in using the MCTDH package.

APPENDIX A: DETAILED STRUCTURE OF THE HAMILTONIAN

The Hamiltonian H_0 corresponding to the overall ground state [see Eq. (4)] takes the following form:

$$H_0 = (T_{\mathrm{vib}} + U_0(x))|0\rangle\langle 0|. \tag{A1}$$

T_{vib} is the vibrational kinetic energy operator and U_0 the PES of longitudinal chain vibrations, with the latter used in the following standard harmonic form:

$$U_0(x) = \sum_m \left[\frac{W}{2}(x_m - x_{m-1})^2 + w_{m0}(x_m - x_{m-1}) \right]. \tag{A2}$$

Its overall minimum defines the ground-state equilibrium configuration which has been abbreviated by x_0.

For the first and second excited manifolds, respectively, the Hamiltonians read

$$H_1 = \sum_{m,n} (\delta_{m,n} H_m + J_{mn})|\phi_m\rangle\langle\phi_n|, \tag{A3}$$

and

$$H_2 = \sum_{k\leq l} \sum_{m\leq n} (\delta_{k,m}\delta_{l,n} H_{mn} + (1 - \delta_{k,m}\delta_{l,n}) J_{kl,mn})|\tilde{\phi}_{kl}\rangle\langle\tilde{\phi}_{mn}|. \tag{A4}$$

H_m and H_{mn} describe chain vibrations for singly and doubly excited states of N–H vibrations,

$$H_m = T_{\mathrm{vib}} + U_0(x) + E_{m1} + (w_{m1} - w_{m0})(x_m - x_{m-1}), \tag{A5}$$

$$\begin{aligned} H_{mn} = {} & T_{\mathrm{vib}} + U_0(x) + \delta_{mn}(E_{m2} + (w_{m2} - w_{m0})(x_m - x_{m-1})) \\ & + (1 - \delta_{mn})(E_{m1} + E_{n1} + (w_{m1} - w_{m0})(x_m - x_{m-1}) \\ & + (w_{n1} - w_{n0})(x_n - x_{n-1})). \end{aligned} \tag{A6}$$

The constants w_{m0}, w_{m1}, and w_{m2} are a measure for the chain vibrational modulation of the N–H excitation energies.

A detailed derivation of the intersite coupling matrix elements J_{mn} and $J_{kl,mn}$, entering the single- and two-exciton Hamiltonians (A5) and (A6), respectively, can be found in Ref. 13. We restrict our model to the case of the nearest-neighbor coupling between the amide units and obtain

$$J_{mn} = -(\delta_{m+1,n} + \delta_{m-1,n})J, \tag{A7}$$

as well as

$$J_{kl,mn} = -\delta_{m,n}\delta_{k,l-1}(\delta_{k,m} + \delta_{l,m})\tilde{J} - \delta_{k,l}\delta_{m,n-1}(\delta_{k,m} + \delta_{k,n})\tilde{J} - (\delta_{k,m}\delta_{l,n-1} + \delta_{k,m}\delta_{l-1,n} + \delta_{l,n}\delta_{k-1,m} + \delta_{l,n}\delta_{k,m-1}) \times (1 - \delta_{k,l})(1 - \delta_{m,n})J. \tag{A8}$$

Here, J denotes the coupling constant referring to the $0 \rightarrow 1$ excitation of one amide unit and a simultaneous $1 \rightarrow 0$ deexcitation of the adjacent unit. The constant $\tilde{J}$ stands for the coupling covering the $1 \rightarrow 2$ excitation and the simultaneous $1 \rightarrow 0$ deexcitation at the nearest-neighbor unit.

The transition dipole operators describing the coupling to the radiation field [Eq. (4)] read

$$\hat{\boldsymbol{\mu}}_{10} = \sum_m \mathbf{d}_1 |\phi_m\rangle\langle 0| \tag{A9}$$

and

$$\hat{\boldsymbol{\mu}}_{21} = \sum_m \mathbf{d}_2 |\tilde{\phi}_{mm}\rangle\langle\phi_m| + \sum_{m\neq n} \mathbf{d}_1 |\tilde{\phi}_{mn}\rangle\langle\phi_m|, \tag{A10}$$

with $\mathbf{d}_1$ and $\mathbf{d}_2$ being responsible for the $0 \rightarrow 1$ and $1 \rightarrow 2$ transitions, respectively, at a given amide unit. All units are described by the same dipole moments oriented parallel to the chain axis. Their magnitude is denoted by d_1 and d_2. To estimate the ratio d_2/d_1 which is only necessary here we assume a linear expansion of the dipole operators with respect to the N–H vibrational normal coordinates Q_m. Thus for a particular amide unit it follows

$$\frac{d_2}{d_1} = \frac{\langle\chi_{m2}|Q_m|\chi_{m1}\rangle}{\langle\chi_{m1}|Q_m|\chi_{m0}\rangle}. \tag{A11}$$

Using a Morse oscillator PES for the N–H vibration[13] one obtains the value $d_2/d_1 = 1.426$.

APPENDIX B: LINEAR ABSORPTION SPECTRUM OF A SINGLE AMIDE UNIT

We calculate the absorption coefficient using the standard formula valid for harmonic systems (see, for example, Ref. 22). To specify the chain motion after the excitation of the amide unit k the vibrational Hamiltonian H_k has to be analyzed [cf. Eq. (A5)] including a PES shifted with respect to the ground-state PES. Denoting the difference between the chain unit m equilibrium coordinate before and after excitation by $\Delta x_m^{(k)} = x_{m1}^{(k)} - x_{m0}$ we obtain in using Eq. (A5) the following:

$$\Delta x_m^{(k)} - \Delta x_{m-1}^{(k)} = -\frac{w_{m1} - w_{m0}}{W}\delta_{m,k} \quad (m = 2,3,\ldots). \tag{B1}$$

The difference between the potential energy minima in both states is as follows:

$$\Delta E^{(k)} = E_{k1} - E_{k0} - \frac{w_{k1}^2 - w_{k0}^2}{2W}. \tag{B2}$$

Assuming the absence of the chain center of mass motion ($\Sigma_m x_m = 0$) and changing to the normal mode coordinates q_ξ,

$$x_m = \frac{1}{\sqrt{M}}\sum_\xi A_{m\xi} q_\xi, \tag{B3}$$

we obtain the following (dimensionless) normal mode displacements:

$$\Delta g_\xi^{(k)} = -\sqrt{\frac{w_\xi}{2\hbar}}(q_{\xi,e}^{(k)} - q_{\xi,g}). \tag{B4}$$

In the Eqs. (B3) and (B4) ω_ξ denote the normal mode frequencies $q_{\xi,e}^{(k)}$, $q_{\xi,g}$ stand for equilibrium normal mode coordinates in the amide excited and ground states, respectively, and $A_{m\xi}$ are transformation coefficients. Then, the linear absorption coefficient corresponding to the single-unit excitation can be written as

$$\alpha_k(\omega) = \frac{2\pi\omega n_{\mathrm{pp}}}{3\hbar c}|d_1|^2 e^{-G(0)} \int dt e^{i(\omega - \Delta E^{(k)}/\hbar)t + G(t) - t/\tau_{\mathrm{deph}}}, \tag{B5}$$

with

$$G(t) = \sum_\xi (\Delta g_\xi^{(k)})^2 e^{-i\omega_\xi t}. \tag{B6}$$

A single Fourier transformation results in the absorbance displayed in Fig. 3.

[1] P. Hamm, M. Lim, and R. M. Hochstrasser, J. Phys. B **102**, 6123 (1998).
[2] S. Woutersen and P. Hamm, J. Chem. Phys. **114**, 2727 (2001).
[3] S. Mukamel and R. M. Hochstrasser, *Multidimensional Spectroscopy, special issue of* Chem. Phys. **266**, 135 (2001).
[4] A. M. Moran, S.-M. Park, J. Dreyer, and S. Mukamel, J. Chem. Phys. **118**, 3651 (2003).
[5] A. G. Dijkstra and J. Knoester, J. Phys. Chem. B **109**, 9787 (2005).
[6] A. C. Scott, Phys. Rep. **217**, 1 (1992).
[7] J. Edler, R. Pfister, V. Pouthier, C. Falvo, and P. Hamm, Phys. Rev. Lett. **93**, 106405 (2004).
[8] V. Pouthier, Phys. Rev. E **68**, 021909 (2003).
[9] V. Pouthier and C. Falvo, Phys. Rev. E **69**, 041906 (2004).
[10] C. Falvo and V. Pouthier, J. Chem. Phys. **122**, 014701 (2005).
[11] C. Falvo and V. Pouthier, J. Chem. Phys. **123**, 184710 (2005).
[12] D. V. Tsivlin and V. May, Chem. Phys. Lett. **408**, 360 (2005).
[13] D. V. Tsivlin, H.-D. Meyer, and V. May, J. Chem. Phys. **124**, 134907 (2006).
[14] T. L. C. Jansen and J. Knoester, J. Phys. Chem. B **110**, 022910 (2006).
[15] T. L. C. Jansen and J. Knoester, J. Phys. Chem. B **124**, 044502 (2005).
[16] H.-D. Meyer, U. Manthe, and L. S. Cederbaum, Chem. Phys. Lett. **165**, 73 (1990).
[17] H.-D. Meyer and G. A. Worth, Theor. Chem. Acc. **109**, 251 (2003).
[18] U. Manthe, H.-D. Meyer, and L. S. Cederbaum, J. Chem. Phys. **97**, 3199 (1992).
[19] M. H. Beck, A. Jäckle, G. A. Worth, and H.-D. Meyer, Phys. Rep. **324**, 1 (2000).
[20] D. M. Alexander and J. A. Krumhansl, Phys. Rev. B **33**, 7172 (1986).
[21] G. A. Worth, M. H. Beck, A. Jäckle, and H.-D. Meyer, The MCTDH Package, Version 8.2 (University of Heidelberg Press, Heidelberg, Germany, 2000); H.-D. Meyer, The MCTDH Package, Version 8.3 (University of Heidelberg Press, Heidelberg, Germany, 2002); see http://www.pci.uni-heidelberg.de/tc/usr/mctdh
[22] V. May and O. Kühn, *Charge and Energy Transfer Dynamics in Molecular Systems*, 2nd ed. (Wiley-VCH, Berlin, 2004).